Optics Letters

Tunable and enhanced optical force with bound state in the continuum

Haoye Qin, Walid Redjem, and Boubacar Kante*

Department of Electrical Engineering and Computer Sciences, University of California, Berkeley, California 94720, USA
**Corresponding author: bkante@berkeley.edu*

Received 16 December 2021; revised 11 February 2022; accepted 24 February 2022; posted 28 February 2022; published 26 March 2022

Light-actuated motors, vehicles, and even space sails have drawn tremendous attention for basic science and applications in space, biomedical, and sensing domains. Optical bound states in the continuum (BIC) are topological singularities of the scattering matrix, known for their unique light-trapping capability and enhanced light–matter interaction. We show that BIC modes enable the generation of enhanced and tunable optical forces and torques. A sharp and controllable line shape is observed in force and torque spectra when approaching high-Q resonance BIC modes. Wavelength and polarization tunability are presented as an effective method to control forces on BIC enclosed structures. Finally finite-size simulations are performed to evaluate the practical applications for a BIC-assisted metavehicle.

https://doi.org/10.1364/OL.451421

Bound states in the continuum (BIC) have attracted considerable interest due to their ability to trap waves within the continuum without radiation loss [1]. First proposed in quantum mechanics, BIC have naturally been extended to optics [2–6]. Especially, periodic optical platforms such as metasurfaces, gratings, and photonic crystal have enabled practical demonstrations and applications of BICs, with high Q-factor and large mode volume [1,7,8]. For instance, BIC have been used for directional and single-mode lasing operation [2,9], biosensing [10,11], and enhancing nonlinear effects [12–14].

Light can exert forces and torques as illustrated in optical tweezers [15] and particle-trapping devices [16,17]. Metasurfaces provide unique opportunities to engineer and manipulate light [18], thus leading to the conception of light-based propulsion for space travel, i.e., laser- and solar-driven spacecraft. Recently, novel studies on optical force have contributed to the proposals of metavehicles [19], plasmonic motors [20–22], dielectric particles [23], self-stabilizing photonic structure for levitation and propulsion [24], and lightsails [25–27] which rely on asymmetric scattering of light. However, metasurfaces showing large tunability and enhancement of optical forces and torques have been missing, while such demonstration could be important in building effective light vehicles/motors/sails with full controllability via properties of incident light.

In this paper, the strong field localization, polarization singularity, and high Q-factor induced by BIC resonance are employed to enhance and tune optical forces and torques, which can directly benefit the development of optically driven transportation. We introduced an asymmetry between two coupled dielectric particles to form a high-Q BIC mode. By controlling the wavelength and/or polarization of the incident light, the generated force and torque can switch direction and intensity, which is useful for on-demand all-optical manipulation. Finally, a realistic finite-size simulation is conducted to quantify the BIC-enhanced and tunable optical forces to control a metavehicle.

The designed metasurface unit cell for BIC mode is shown in Fig. 1(a). Two silicon bars with the same width (200 nm) and length L_1 (fixed at 280 nm) and L_2 are placed in free space. The gap between the two bars is 75 nm and their thickness is 250 nm. Periodic boundary conditions are applied in x and y directions. L_2 can be tuned to change the asymmetry ratio defined as $\alpha = (L_1 - L_2)/L_2$ [28]. When $\alpha = 0$, in-plane symmetry is fulfilled, and a BIC mode is present. Reducing the length of one of the bars breaks the in-plane symmetry and leads to a quasi-BIC mode with a sharp spectral resonance. To investigate the optical force and torque associated with the high-Q quasi-BIC mode, we integrated the Maxwell stress tensor (MST) around a box enclosing the unit cell [Fig. 1(a)]. The expressions used for calculating the time-averaged force **F** and torque **Tor** are given by

$$\mathbf{F} = \iint_S (\mathbb{T} \cdot \boldsymbol{n}) \mathrm{dS}, \tag{1}$$

$$\mathbf{Tor} = \iint_S \boldsymbol{r} \times (\mathbb{T} \cdot \boldsymbol{n}) \mathrm{dS}, \tag{2}$$

where S is the surface of the MST box, $\boldsymbol{n}$ is the unit vector normal to the surface, and $\boldsymbol{r}$ is the position vector regarding the original point. $\mathbb{T}$ is the stress tensor with matrix elements defined as

$$\mathbb{T}_{ij} = \epsilon_0 \left(E_i E_j - \frac{1}{2} |\mathrm{E}|^2 \delta_{ij} \right) + \frac{1}{\mu_0} \left(B_i B_j - \frac{1}{2} |\mathrm{B}|^2 \delta_{ij} \right), \tag{3}$$

where E_i and B_i are the ith components of the electric and magnetic field, respectively. In the following we used the finite-element method to simulate the electromagnetic field and Eqs. (1)–(3) to calculate the optical forces.

Figures 1(b)–1(d) illustrate the optical response of the metasurface with two asymmetric particles as a unit cell. In Fig. 1(b), the evolution of the transmission spectrum is shown for different asymmetry ratios. As expected, at $\alpha = 0$, in-plane symmetry

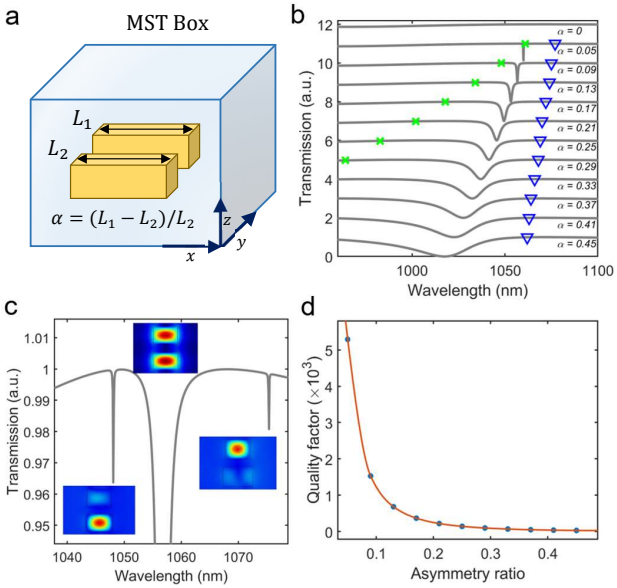

Fig. 1. Schematic and optical response of coupled particles exhibiting a BIC mode for enhanced optical force and torque. (a) Schematic view of the asymmetric silicon bars with length L_1 (fixed at 280 nm) and L_2. Both bars have a width of 200 nm. The gap between them is 75 nm and their common thickness is 250 nm. The asymmetry ratio α is defined as $\alpha = (L_1 - L_2)/L_1$. Periodic boundary condition is applied in x and y directions with lattice constants $p_x = 725$ nm and $p_y = 530$ nm, respectively. (b) Transmission spectra for different asymmetry ratios. The dip corresponds to the quasi-BIC mode whereas the cross and triangle correspond to individual modes 1 and 2 shown in (c). (c) Enlarged view of the two individual quasi-BIC modes with $\alpha = 0.09$ in (b). Corresponding distribution of magnetic field for individual quasi-BIC modes 1 and 2 and for the collective quasi-BIC mode is shown. For individual modes, the field is localized in either the top or bottom particle. The bottom of the middle dip is omitted for better view. (d) Quality factor as a function of asymmetry ratio for the collective mode. The dots are the extracted quality factor through rational fitting. The line is an exponential fit.

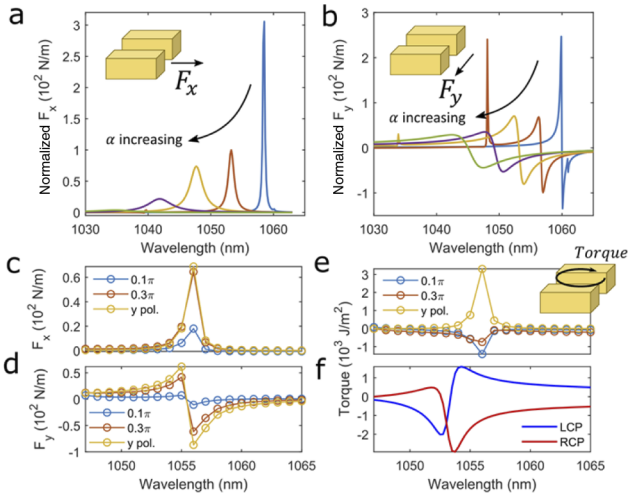

Fig. 2. Optical force in (a) x and (b) y directions as a function of wavelength for different asymmetry ratios [0.05 (first from the right), 0.09 (second), 0.13 (third), 0.17 (fourth) and 0.21 (fifth)]. The forces calculated from MST box are normalized to the period of the unit cell. Inset shows the generated optical force in x direction. Optical force (c) F_x and (d) F_y with $\alpha = 0.13$ for different polarization of the incident light. The optical force can be switched from positive to negative via tuning the incident light wavelength and force intensity via polarization angle. Optical torque for different polarization states: (e) linear polarization with different polarization angles; (f) evaluation of optical torque under LCP and RCP incident light.

produces a symmetry-protected BIC mode with disappeared linewidth. Increasing α leads first to a sharp resonance dip with decreasing quality factor, illustrated by the broadened and blue-shifted resonance. Cross (individual mode 1) and triangle (individual mode 2) markers in Fig. 1(b) indicate the wavelength evolution of two individual modes versus the change of asymmetry ratio. Figure 1(d) shows the exponentially decreasing Q-factor of the collective mode extracted using a rational fit method for the complex scattering parameter S_{21}. An interesting phenomenon accompanied by the "visible" collaborative quasi-BIC mode is that two individual quasi-BIC modes have emerged. The two modes can be seen in the enlarged view of the spectrum [Fig. 1(c)], featuring sharp line shape They arise from the in-plane symmetry of an individual particle instead of the two interactive particles and are then perturbed by the mode coupling to reveal a quasi-BIC feature. The individual mode 2 is more sensitive to the asymmetry ratio because it corresponds to the resonator that is tuned in dimension. Corresponding magnetic field profiles for individual modes 1 and 2 plotted in Fig. 1(c) confirm the mode localization in only one particle. The near-field distribution of the magnetic field for the collaborative quasi-BIC mode is presented in the top inset of Fig. 1(c) and the strongly confined field profile indicates a high-Q resonance. It is named a collaborative mode as there is a clear interaction between the two resonant particles.

In Figs. 2(a) and 2(b), with a plane-wave illumination, a strong enhancement of optical forces F_x and F_y assisted by the high-Q resonance of the quasi-BIC mode is shown at the same time when the structure has a small asymmetry. Here we refer to the enhancement compared with when the quasi-BIC structure is far from resonant wavelength. The force is calculated under an incident power of 1 $\mu W/\mu m^2$. For $\alpha = 0.05$ the optical force is ten times larger than for $\alpha = 0.20$. As the asymmetry ratio increases, the optical force reduces exponentially. In addition, tunability can be achieved by sweeping the incident light wavelength. There exists a sharp peak switch from positive to negative F_y and crossing zero exactly at the BIC resonance. This is better seen in Fig. 2(d) showing the optical force F_y around the BIC resonance (1055 nm). The positive to negative feedback region is due to the asymmetry of the field along the xz plane that induces a force along y [see Eq. (3)]. At the BIC wavelength the field is symmetric, thus F_y is null. Tunability of optical forces and torques can also be achieved through varying the polarization of the incident light. Figures 2(c) and 2(d) demonstrate the effect of polarization on optical forces for a given asymmetry ratio of 0.05. Changing the polarization from 0.1π to an angle of 0.3π and y polarization results in increasing the BIC-induced force. Figures 2(e) and 2(f) present the tailorable optical torque of the metasurface calculated from Eq. (2) under illumination of different polarization states. The direction of the torque can be tuned with the wavelength and the polarization angle. The structure is tolerant to polarization changes when it is varied

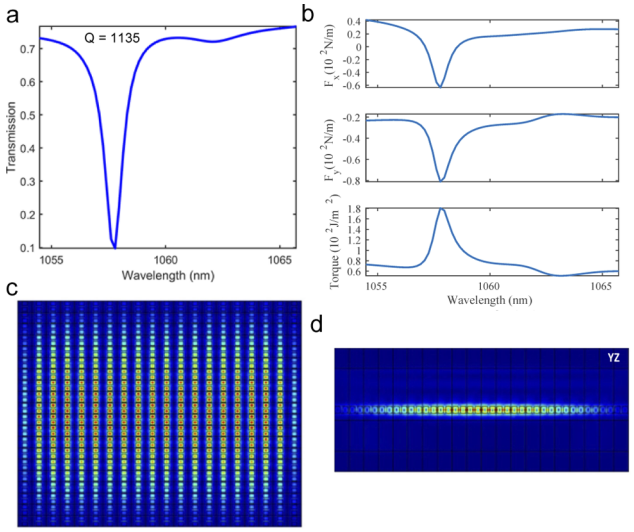

Fig. 3. Proposed metamotor on glass substrate. (a) Transmission spectrum from finite-size simulation showing a Q-factor of 1135. (b) Calculated optical force and torque from finite-size simulation. (c) Top view and (d) side view showing the electric field distribution of the corresponding quasi-BIC mode present in the transmission spectra.

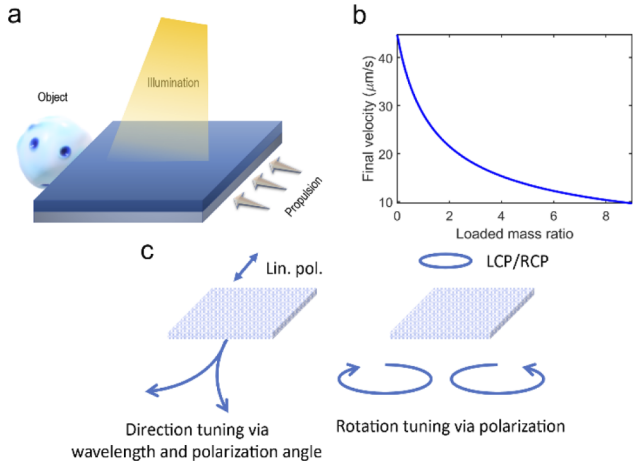

Fig. 4. (a) Schematic of the BIC-assisted metavehicle with a nano-object in front of the metavehicle for use in transportation and delivery using optical propulsion. (b) Estimated final-state velocity for propulsion in y direction as a function of additional loaded mass of the propulsed nano-object with an incident power of 1 $\mu W/\mu m^2$. The loaded mass is given in terms of unloaded mass of the metavehicle. (c) Tunability of the BIC-assisted metavehicle for controlling moving direction and rotation via wavelength, polarization angle, and polarization state.

0.3π from the y direction. The generated optical force is nearly the same while the direction of rotation changes, allowing full control of the structure's rotation, angular position, and linear motion. The effect of circular polarized light (left, LCP; right, RCP) is evaluated in Fig. 2(f). A switch from LCP to RCP also symmetrically switches the direction of the torque, hence the direction of rotation.

The general idea of BIC-enhanced generational of optical force and torque has been demonstrated with a dielectric metasurface, which can be transferred for applications in a metavehicle [19], lightsail in space [24,27,29], and optical tweezers. The BIC enhancement can benefit ultra-light spacecraft and even laser-propelled lightsails for space exploration with enhanced moving velocity and steering capability. As for metavehicles, a practical design with 20×20 unit cells on glass substrate is now investigated. The finite-size structure comprises a bottom layer of glass with 0.5 μm thickness and previously studied asymmetric particles with asymmetry ratio of 0.09. The substrate thickness is chosen to reduce total mass and, for experimental feasibility, the metavehicle can be fabricated with a twice electron-beam lithography process [19,22]. Simulated transmission depicted in Fig. 3(a) shows a quasi-BIC resonance dip corresponding to a Q-factor of 1135, which is comparable with the Q-factor of 1528 previously extracted from an asymmetric infinite structure [Fig. 1(d)]. This relatively small reduction is due to additional scattering losses at the boundaries of the finite structure. The top view and side view of this quasi-BIC mode are presented in Figs. 3(c) and 3(d) with electrical field distribution. The mode is highly localized within the central nanobars and along one direction due to the asymmetry of the unit cells. We can observe scattering mainly at the right-hand edges of the structure where the field is stronger, which explains the reduction of Q-factor mentioned above. Figure 3(b) shows the enhancement and tunability of optical forces and torques. The intensity of the forces is comparable to the case of the infinite periodic metasurface.

To investigate the metasurface as an optical motor in water, we assume that only the friction coming from the bottom surface of the metavehicle is present and we neglect the frontal area friction because of its large length-to-thickness ratio (20:1). Thus, under the laminar flow approximation, the total drag coefficient can be estimated from the local skin coefficient:

$$C_D = \frac{1}{bL}\int_0^L 0.664\left(\frac{U}{\nu}\right)^{-0.5} x^{-0.5} b\,\mathrm{d}x = 1.33\left(\frac{\nu}{UL}\right)^{0.5} \quad (4)$$

or

$$C_D = \frac{1.33}{\sqrt{\mathrm{Re}_L}}, \quad (5)$$

where $Re_L = UL/\upsilon$ is called the Reynolds number, and U, L, b, and ν represent the flow velocity, length, depth of the metasurface, and kinematic viscosity of the flow, respectively [29]. For water at room temperature, $\nu = 8.917 \times 10^{-7} \mathrm{m}^2/\mathrm{s}$ resulting in $Re_L = 16.26U$ and $C_D = 0.3798/\sqrt{U}$ for propulsion in the y direction. Figure 4(a) shows a schematic of the metasurface with BIC-enhanced and tunable optical forces applied to the metavehicle for transportation and delivery. An object is loaded in front of the metavehicle to illustrate its carrying capacity, which avoids influencing the optical properties of quasi-BIC. Using Eq. (5) for the drag coefficient and assuming a balanced force at final state, the achieved velocity with optical propulsion in the y direction and with an incident power of 1 $\mu W/\mu m^2$ is evaluated for different loaded mass ratio – corresponding to the ratio between the loaded mass and the mass of the metavehicle [Fig. 4(b)]. The object like a single cell has a similar size to the frontal height of the metavehicle. Due to the high Q-factor and large force enhancement, our proposed device can move relatively fast even with a loaded mass comparable to or larger than the mass of the vehicle. The estimated loaded mass is 2.46 ng for the ratio of 6. Finally, Fig. 4(c) presents the tunability of

the metavehicle for controlling the direction of motion and rotation via wavelength, polarization angle, and polarization state as illustrated in Figs. 2 and 3.

We have proposed the incorporation of quasi-BIC modes into metasurfaces for enhancing the optical forces and torques with large tunability. By changing the asymmetry of the two-bar structure, high-Q quasi-BIC modes are shown to enhance forces in x and y directions and the torque in the z direction. Along with this enhancement, wavelength and polarization tuning of force/torque directions can be realized. Finally, finite-size simulations showed that even a relatively small structure can be an efficient metavehicle. Hence, the proposed metasurface may contribute to on-demand control of light vehicles/motors/sails for applications in space exploration, medicine, sensing, and actuators by only modulating the properties of incident light.

Acknowledgment. The project was supported by the Starshot–Breakthrough Initiatives, the Office of Naval Research Young Investigator Award (N00014-17-1-2671), and National Science Foundation Career Award (ECCS-1554021).

Disclosures. The authors declare no conflicts of interest.

Data availability. Data underlying the results presented in this paper are not publicly available at this time but may be obtained from the authors upon reasonable request.

REFERENCES

1. C. W. Hsu, B. Zhen, A. D. Stone, J. D. Joannopoulos, and M. Soljacic, Nat. Rev. Mater. **1**, 16048 (2016).
2. A. Kodigala, T. Lepetit, Q. Gu, B. Bahari, Y. Fainman, and B. Kanté, Nature **541**, 196 (2017).
3. C. W. Hsu, B. Zhen, J. Lee, S. L. Chua, S. G. Johnson, J. D. Joannopoulos, and M. Soljačić, Nature **499**, 188 (2013).
4. X. Zhao, C. Chen, K. Kaj, I. Hammock, Y. Huang, R. D. Averitt, and X. Zhang, Optica **7**, 1548 (2020).
5. T. Lepetit and B. Kante, Phys. Rev B **90**, 241103 (2014).
6. Y. Plotnik, O. Peleg, F. Dreisow, M. Heinrich, S. Nolte, A. Szameit, and M. Segev, Phys. Rev. Lett. **107**, 183901 (2011).
7. K. Koshelev, Y. Tang, K. Li, D. Y. Choi, G. Li, and Y. Kivshar, ACS Photonics **6**, 1639 (2019).
8. D. C. Marinica, A. G. Borisov, and S. V. Shabanov, Phys. Rev. Lett. **100**, 183902 (2008).
9. C. Huang, C. Zhang, S. Xiao, Y. Wang, Y. Fan, Y. Liu, N. Zhang, G. Qu, H. Ji, J. Han, L. Ge, Y. Kivshar, and Q. Song, Science **367**, 1018 (2020).
10. A. Tittl, A. Leitis, M. Liu, F. Yesilkoy, D. Y. Choi, D. N. Neshev, Y. S. Kivshar, and H. Altug, Science **360**, 1105 (2018).
11. A. Ndao, L. Shu, W. Cai, J. Ha, J. Park, R. Contractor, Y. Lo, and B. Kanté, Nanophotonics **9**, 5 (2020).
12. N. Bernhardt, K. Koshelev, S. J. U. White, K. W. C. Meng, J. E. Fröch, S. Kim, T. T. Tran, D. Y. Choi, Y. Kivshar, and A. S. Solntsev, Nano Lett. **20**, 5309 (2020).
13. L. Carletti, K. Koshelev, C. De Angelis, and Y. Kivshar, Phys. Rev. Lett. **121**, 033903 (2018).
14. K. Koshelev, A. Bogdanov, and Y. Kivshar, Sci. Bull. **64**, 836 (2019).
15. K. B. Crozier, Light: Sci. Appl. **8**, 35 (2019).
16. J. C. Ndukaife, A. V. Kildishev, A. G. A. Nnanna, V. M. Shalaev, S. T. Wereley, and A. Boltasseva, Nat. Nanotechnol. **11**, 53 (2016).
17. D. Gao, W. Ding, M. Nieto-Vesperinas, X. Ding, M. Rahman, T. Zhang, C. T. Lim, and C. W. Qiu, Light: Sci. Appl. **6**, e17039 (2017).
18. D. Neshev and I. Aharonovich, Light: Sci. Appl. **7**, 58 (2018).
19. D. Andrén, D. G. Baranov, S. Jones, G. Volpe, R. Verre, and M. Käll, Nat. Nanotechnol. **16**, 970 (2021).
20. O. Ilic, I. Kaminer, B. Zhen, O. D. Miller, H. Buljan, and M. Soljačić, Sci. Adv. **3**, 1 (2017).
21. Z. Zhan, F. Wei, J. Zheng, W. Yang, J. Luo, and L. Yao, Nanotechnol. Rev. **7**, 555 (2018).
22. M. Liu, T. Zentgraf, Y. Liu, G. Bartal, and X. Zhang, Nat. Nanotechnol. **5**, 570 (2010).
23. E. N. Bulgakov and A. F. Sadreev, Opt. Lett. **45**, 5315 (2020).
24. O. Ilic and H. A. Atwater, Nat. Photonics **13**, 289 (2019).
25. W. Jin, W. Li, M. Orenstein, and S. Fan, ACS Photonics **7**, 2350 (2020).
26. K. V. Myilswamy, A. Krishnan, and M. L. Povinelli, Opt. Express **28**, 8223 (2020).
27. H. A. Atwater, A. R. Davoyan, O. Ilic, D. Jariwala, M. C. Sherrott, C. M. Went, W. S. Whitney, and J. Wong, Nat. Mater. **17**, 861 (2018).
28. K. Koshelev, S. Lepeshov, M. Liu, A. Bogdanov, and Y. Kivshar, Phys. Rev. Lett. **121**, 193903 (2018).
29. F. M. White, *Fluid Mechanics*, 7th ed. (McGraw Hill, 2011).